ELSEVIER

Chemical Geology 240 (2007) 313–325

CHEMICAL GEOLOGY
INCLUDING
ISOTOPE GEOSCIENCE

www.elsevier.com/locate/chemgeo

Mercury mobilization by oxidative dissolution of cinnabar (α-HgS) and metacinnabar (β-HgS)

Elizabeth A. Holley [a,*], A. James McQuillan [b], Dave Craw [a], Jonathan P. Kim [b], Sylvia G. Sander [b]

[a] *Geology Department, University of Otago, P.O. Box 56, Dunedin, New Zealand*
[b] *Chemistry Department, University of Otago, P.O. Box 56, Dunedin, New Zealand*

Received 6 December 2006; received in revised form 23 February 2007; accepted 3 March 2007

Editor: D. Rickard

Abstract

Cinnabar (α-HgS) and metacinnabar (β-HgS) dissolved at environmentally significant rates in oxygenated slurry experiments simulating a low-flow fluvial system. Based on SO_4^{2-} production, cinnabar dissolution rates were 2.64 to 6.16 μmol (SO_4^{2-}) m^{-2} day^{-1}, and metacinnabar dissolution rates were 1.20 to 1.90 μmol (SO_4^{2-}) m^{-2} day^{-1}. Monodentate-bound thiosulfate ($S_2O_3^{2-}$) was identified as an oxidation product on the HgS surface by ATR-IR spectroscopy based on strong infrared absorption bands in the 1140–1145 cm^{-1} and 1006–1014 cm^{-1} regions. The presence of sulfide oxidation intermediates on the HgS surface indicates that SO_4^{2-} concentration underestimates α-HgS and β-HgS dissolution in this setting. Mercury release rates during dissolution were more than two orders of magnitude less than SO_4^{2-} production, but were significant: 0.47 mg (Hg) m^{-2} y^{-1} from cinnabar [6.45 nmol (Hg) m^{-2} day^{-1}], and 0.17 mg (Hg) m^{-2} y^{-1} from metacinnabar [2.29 nmol (Hg) m^{-2} day^{-1}]. The Hg mobilized during α-HgS and β-HgS dissolution is sufficient to form natural Au–Hg amalgam in downstream placer settings. The proportion of mercury that is not remobilized during α-HgS and β-HgS dissolution likely adsorbs to the dissolving mercuric sulfide. Adsorption of Hg^{2+} to cinnabar was detected in situ by anodic stripping voltammetry using a cinnabar-modified carbon paste electrode following accumulation of Hg^{2+} on the electrode at open circuit potential.

Keywords: Sulfide solubility; Mercury; Gold; Thiosulfate; Adsorption; Infrared

1. Introduction

Mercury (Hg) is a widespread contaminant that is hazardous to aquatic and terrestrial ecosystems (EPA, 1997). The bioavailability and toxicity of Hg are governed by its speciation (Kim et al., 2004). Natural and anthropogenic processes contribute to the global redistribution of Hg from natural deposits into the surrounding environment (Lacerda, 1997). Mercuric sulfide (HgS) is an important component of the Hg cycle. Cinnabar (α-HgS: red, hexagonal) is the primary ore in most of the world's twenty-six Hg mineral belts (Rytuba, 2003). Cinnabar ore is processed by roasting, during which the resulting Hg^0 vapors are condensed and trapped. Cinnabar is transformed to its polymorph

* Corresponding author. Tel.: +64 408 356 6193.
E-mail address: lizholley@gmail.com (E.A. Holley).

0009-2541/$ - see front matter © 2007 Elsevier B.V. All rights reserved.
doi:10.1016/j.chemgeo.2007.03.001

metacinnabar at 345 °C (β-HgS: black, cubic) (Dickson and Tunell, 1959). Host rock cations such as iron and zinc are incorporated into the HgS crystal structure during ore roasting, preventing the mercuric sulfide from returning to its original hexagonal form (Tauson and Akimov, 1997). The predominant Hg species in wastes at Hg mine sites are primary cinnabar in discarded low-grade ore, and secondary metacinnabar in tailings (Kim et al., 2004). Metacinnabar also occurs in primary deposits and authigenically in Hg-contaminated floodplains and soils. Precipitation of this mineral has been documented due to atmospheric Hg deposition in the Florida Everglades (Ravichandran et al., 1999). Mercury dissolves out of anthropogenic Hg–Au amalgams formed during gold mining and reprecipitates as authigenic metacinnabar at the Carson River Superfund Site, Nevada (Lechler et al., 1997).

Cinnabar has been shown to be sparingly soluble in acidic mine drainage waters (Burkstaller et al., 1975) and in sulfidic solutions approximating natural anoxic waters (Paquette and Helz, 1995). Ravichandran et al. (1999) showed that β-HgS precipitation was inhibited by dissolved organic matter (DOM) in anoxic experiments. Dissolved organic matter enhances Hg release from cinnabar (Ravichandran et al., 1998; Waples et al., 2005), and measured Hg release rates in the presence of DOM ranged from 2.00×10^{-2} to 6.19×10^{-1} μmol (Hg) mg $(C)^{-1}$ m^{-2} day^{-1} (Waples et al., 2005). Metacinnabar dissolution has been measured in batch experiments under oxidative conditions using sulfate production as a proxy, and reported rates vary from 3.15×10^{-2} to 5.87×10^{-2} μmol (SO_4^{2-}) m^{-2} day^{-1} (Barnett et al., 2001). However, Hg release rates were 1 to 3 orders of magnitude less than SO_4^{2-} in that study.

It has been proposed that Hg^{2+} adsorbs to the surface of HgS during HgS dissolution (Burkstaller et al., 1975; Barnett et al., 2001), resulting in stoichiometrically unequal release of Hg and S to solution. Support for this hypothesis has relied on solution chemistry of filtered samples to illustrate incomplete recovery of Hg^{2+} added to batch experiments. This type of analysis necessitates separation of the solution and the solid phase, which disrupts the experimental equilibrium and does not account for the influence of suspended colloidal material. Adsorption of Hg^{2+} to Fe- and Al-(hydr) oxides and soil humic fractions has been detected in situ by synchrotron-based molecular spectroscopic methods (Collins et al., 1999; Xia et al., 1999; Kim et al., 2004), and Walcarius et al. (1999) have detected Hg^{2+} adsorption to pyrite in situ by voltammetry. To date there has been no reported in situ analysis of Hg^{2+} adsorption to HgS.

In this work we have examined cinnabar and metacinnabar dissolution in a simulated fluvial system using oxygenated batch reactor experiments. We have extended the previous studies of mercuric sulfide solubility in aquatic environments by conducting the first direct comparison of α-HgS and β-HgS solubility. We have assessed the formation of sulfide oxidation intermediates such as thiosulfate ($S_2O_3^{2-}$) on the mercuric sulfide surface using Attenuated Total Reflection Infrared (ATR-IR) spectroscopy of thin particle films of batch reactor α-HgS and freshly precipitated HgS. Based on spectral and batch reactor data, we have evaluated the suitability of sulfate as a proxy for HgS dissolution. We have also monitored Hg concentration in batch reactor dissolution experiments and compared the release of Hg from cinnabar and metacinnabar to the release of sulfur. The dissolution of mercuric sulfides has implications for Hg mobility in catchments hosting mined and unmined cinnabar deposits, and catchments containing authigenic metacinnabar resulting from atmospherically-deposited or gold mining related Hg. The fate of Hg released from HgS was examined in the context of Au–Hg amalgamation and Hg^{2+} adsorption to HgS. The potential was assessed for mercuric sulfide-derived Hg to amalgamate with Au in the presence of a suitable reducing agent. Adsorption of Hg^{2+} to cinnabar was detected in situ by anodic stripping voltammetry using a cinnabar-modified carbon paste electrode. These processes have important environmental implications for the immobilization of HgS-derived Hg.

2. Experimental methods

2.1. Batch HgS solubility experiments

Slurries of cinnabar and metacinnabar were sparged with air and agitated in order to approximate the conditions experienced by detrital α-HgS and β-HgS. Four experiments were conducted to compare α-HgS and β-HgS solubility. Experiment A was a slurry of 0.43 M α-HgS in deionized water. Experiment B was a comparison of 0.1 M α-HgS and 0.1 M β-HgS slurries in deionized water. Experiments C and D were both comparisons of 0.1 M α-HgS and 0.1 M β-HgS slurries in natural river water. Each experiment included a second set of batch reactors containing gold foil in addition to the reagents listed above. Experimental conditions are also listed in Table 1 for convenience.

Powdered reagent-grade pure cinnabar (Riedel-de Haën) and metacinnabar (Aldrich) were used in order to prevent introduction of other metals into the experiment, as natural cinnabar ore commonly contains up to

4600 ppm of other metals (Rytuba and Klein, 1986). Brunauer–Emmett–Teller (BET) N_2 adsorption surface areas were 1.28±0.06 $m^2\ g^{-1}$ for α-HgS and 2.76± 0.04 $m^2\ g^{-1}$ for β-HgS. Deionized water was 18.2 MΩ cm^{-1} (Millipore, Milli-Q). Natural river water was collected from the Leith Stream (Dunedin, New Zealand) during normal flow conditions using trace metal clean techniques. Gold was in the form of five 50 mg pieces of foil that had been heated to 500 °C for 24 h to remove any Hg. Electron microprobe analyses indicated that the foil was pure Au containing <0.1 wt.% Ag and <0.2 wt.% Hg (detection limits). In experiments B–D (see Table 1 for conditions), the Au was contained in Medicell dialysis tubing with a pore diameter of 2.5 nm. Experiments were conducted in 500 mL glass conical flasks with glass spargers and blown glass frets. Glassware was prepared by soaking overnight in AR grade concentrated HNO_3. Flasks were anchored in the moving portion of a Julabo SW22 shaking water bath set to 100 rpm and 24 °C. Back-and-forth agitation of the flasks was achieved using the automated setting of the water bath, rather than magnetic stirring devices which could cause grinding of HgS particles. Instrument grade compressed air was constantly bubbled through the spargers at 50 mL min^{-1}, and spargers were fully submerged throughout the duration of the experiment. Air residence time was 10 min in the 500 mL flasks, in contact with 250 mL of slurry. Under these sparging conditions, 1.7 mM O_2 (55 mg $O_2\ L^{-1}$) was provided to the experiment, which should sufficiently exceed concentrations necessary for 100% dissolved O_2 saturation.

Immediately prior to sampling, batch reactors were agitated vigorously by hand for 1 min, and then allowed to settle for 1 min. No difference in results was observed when this procedure was omitted or varied in duration. All aqueous samples were <0.45 μm filtrates and were stored at 4 °C in plastic sample vials unless otherwise noted. Dissolution was monitored by SO_4^{2-} production according to the reaction for oxidative β-HgS dissolution proposed by Barnett et al. (2001), who observed complete oxidation of sulfide to sulfate under similar conditions:

$$HgS(s) + 2O_2(aq) + 2H_2O \leftrightarrow Hg(OH)_2(aq) + SO_4^{2-} + 2H^+$$

Mercury concentration was monitored in aqueous samples in experiments B and C (Table 1). In experiment C, Hg samples (7 mL) were immediately preserved with 100 μL of AR grade BrCl and stored in Teflon sample vials.

Oxidation of S^{2-} to SO_4^{2-} was investigated by reanalyzing samples for SO_4^{2-} 3 weeks after collection and 6 weeks after collection, and by treatment of samples with H_2O_2. Batch reactor pH was monitored in experiments C and D using a three point calibration. In experiment C (see Table 1 for conditions), Hg lost from the system by volatilization was trapped on Au-coated quartz sand sample columns at the sparger outlets. Total predicted losses for the experiment were calculated based on these data. In experiments C and D, an additional 50 mg piece of Au foil was added to the experiment in dialysis tubing for 1 h. The total amount of Hg detected on this Au was used to extrapolate to the amount of Hg predicted to be associated with the Au in each reactor. In these calculations it was assumed that reactive surface area placed no limitations on Hg sorption to or amalgamation with Au, and results represent the maximum possible amount of Au-associated Hg.

Table 1
Batch reactor starting conditions, final quantity of sulfate in batch reactors, and total mercury detected in aqueous, gold foil, and volatilized samples

Batch experiment	Slurry [HgS]/M	Experimental conditions	Final SO_4^{2-}/μmol	Max Hg(aq)/μmol	Hg (Au)/μmol	Hg (vol)/μmol
A1: α-HgS	0.43	Deionized H_2O	5.75×10^{1}	–	–	–
A2: α-HgS	0.43	Deionized H_2O+Au	6.09×10^{1}	–	–	–
B1: α-HgS	0.1	Deionized H_2O	9.93×10^{1}	3.6×10^{-2}	–	–
B2: α-HgS	0.1	Deionized H_2O+Au	1.19×10^{2}	1.1×10^{-5}	–	–
B3: β-HgS	0.1	Deionized H_2O	1.96×10^{2}	1.3×10^{-5}	–	–
B4: β-HgS	0.1	Deionized H_2O+Au	1.91×10^{2}	1.6×10^{-5}	–	–
C1: α-HgS	0.1	River H_2O	5.01×10^{1}	1.2×10^{-2}	–	5.0×10^{-2}
C2: α-HgS	0.1	River H_2O+Au	1.07×10^{2}	4.0×10^{-2}	3.8×10^{-6}	–
C3: β-HgS	0.1	River H_2O	6.10×10^{1}	2.7×10^{-3}	–	1.0×10^{-1}
C4: β-HgS	0.1	River H_2O+Au	5.47×10^{1}	7.1×10^{-3}	4.7×10^{-6}	–
D1: α-HgS	0.1	River H_2O	5.74×10^{1}	–	–	–
D2: α-HgS	0.1	River H_2O+Au	5.82×10^{1}	–	8.1×10^{-7}	–
D3: β-HgS	0.1	River H_2O	5.36×10^{1}	–	–	–
D4: β-HgS	0.1	River H_2O+Au	5.10×10^{1}	–	7.9×10^{-7}	–

2.2. Batch experiment analytical techniques

Aqueous samples were analyzed for SO_4^{2-} by ion chromatography. The system was calibrated according to a Na_2SO_4 standard. A 0.104 mM standard was analyzed each day to confirm accuracy. Duplicates analyzed at the end of the run were within 2.1 μM. In experiment A, analyses were provided by Chemsearch Laboratory (University of Otago).

Gold foil in experiments C and D (Table 1) was prepared for Hg analysis by pyrolysis in a gas train, during which the Hg was removed from the Au and collected on Au-coated quartz sand sample columns. Aqueous samples in experiments B and C were prepared for Hg analysis by BrCl oxidation followed by $SnCl_2$ reduction, gas phase stripping, and collection of Hg on Au-coated quartz sand sample columns. Oxidation by BrCl was omitted for pre-treated samples in experiment C.

Mercury trapped on sample columns from Au foil (experiments C, D), aqueous samples (B, C), and volatilization (C) was quantified by two-stage Au amalgamation in a gas train in line with a cold-vapor atomic fluorescence spectrophotometer (CVAFS) according to the method of Gill and Fitzgerald (1987). Detection limit was 1.5 nM with an analytical precision of 10% (Gill and Fitzgerald, 1987; Gill and Bruland, 1990).

2.3. ATR-IR spectroscopy

Attenuated Total Reflection Infrared (ATR-IR) spectroscopy was employed in order to observe surface species rather than the bulk HgS itself. Mercuric sulfide has Hg–S stretch absorptions at low wavenumber, but these are not within the spectral range examined here. Experiments were conducted using a 45° ZnSe single internal reflection ATR prism (Harrick Scientific). The prism was polished with a 0.015 μm aqueous alumina powder suspension and a Buehler polishing microcloth prior to use. Contact between the film and an aqueous phase was achieved by placing an O-ring and a perspex flow cell on the prism. Tygon tubing was used to pump solutions through the cell using a Masterflex pump (Fig. 1).

A particle film was prepared from a 100-fold dilution of α-HgS slurry extracted from the B1 batch reactor at the conclusion of that experiment. A 250 μL aliquot of this material was applied to the ZnSe prism. For comparison, fresh mercuric sulfide was prepared by rapid addition of 1 mL of 2×10^{-3} M Na_2S (Aldrich) to 1 mL of 2×10^{-3} M $HgCl_2$ (AnalaR) during constant stirring. After 5 min, 250 μL of the resulting sol was applied to the ZnSe prism. Films were dried for 30 min

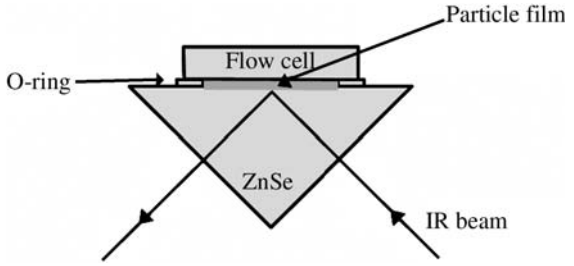

Fig. 1. ATR-IR spectroscopy experimental setup showing 45° ZnSe prism coated with a particle film. Solutions are pumped through the flow cell and over the film.

in a water pump vacuum desiccator. Deionized water (Millipore, Milli-Q) was used for all infrared procedures and solutions, and all reagents were AR grade. X-ray diffraction analysis (XRD) indicated that the HgS was predominately amorphous.

Infrared spectra were obtained using a Digilab FTS4000 spectrometer equipped with a DTGS detector and a FastIR accessory (Harrick Scientific). The optical bench was purged with dried air. Data were recorded using Digilab Merlin software version 3.4. Spectra were determined at 4 cm^{-1} resolution over 64 scans, and data were recorded from 4000 to 800 cm^{-1}. Infrared spectra were collected for dry HgS films using the bare prism as a reference spectrum.

The presence of adsorbed $S_2O_3^{2-}$ was examined in a multi-step flow experiment, during which all solutions were pumped over the film at 1 mL min^{-1}. Adsorbed $S_2O_3^{2-}$ was removed from the film by contact with water, 10^{-3} M NaOH, and water again for 20 min each. A 10^{-3} M $Na_2S_2O_3$ solution (Scientific Supplies Ltd.) was pumped over the HgS film for 1 h. Thiosulfate adsorption from the solution to the film was monitored by the infrared absorbance in the 1140–1171 cm^{-1} and 1004–1014 cm^{-1} regions. Loss of newly adsorbed $S_2O_3^{2-}$ was monitored during the contact of the film with water for 1 h. Spectra were collected at 5 min intervals. The reference was the final spectrum collected during contact with the solution in each previous experimental step.

2.4. Voltammetric detection of Hg^{2+} adsorption to α-HgS

Adsorption of Hg^{2+} was compared among experiments with a pure carbon paste electrode, a cinnabar-modified carbon paste electrode, and a silica-modified carbon paste electrode. Electrodes were prepared using oil-based carbon paste (Bioanalytical Systems Inc.), or by mixing 0.9 g of the paste with either 0.1 g of cinnabar (see Section 2.1) or 0.1 g of amorphous silica gel (Merck

Kieselgel 60; 450–520 $m^2\ g^{-1}$ by BET N_2 adsorption). Metacinnabar is significantly more conductive than cinnabar and has been utilized in pure form as an electrode (Brandon et al., 2001), and for this reason it was not used as an electrode modifier in the present experiment. The electrode material was packed firmly into a polychlorotrifluoroethylene (CTFE) tube with a brass rod contact and having a 3 mm internal diameter. The electrode was polished on a clean glass surface. The Hg^{2+} solutions were made up from a 4.98 mM $HgNO_3$ standard (Merck). Cyclic voltammograms and anodic stripping voltammograms were collected in 0.2 M quartz distilled HNO_3. Deionized water (Millipore, Milli-Q) was used for all preparations and procedures.

Electrochemical measurements were made using an Eco Chemie μAutolab II, a 663 VA Metrohm electrode stand, and an Eco Chemie IME 663 interface. Experiments were monitored and controlled by Autolab GPES software (Eco Chemie). The working electrode was the unmodified or modified carbon paste electrode. A glassy carbon rod counter electrode and an Ag/AgCl (3 M KCl) reference electrode were used. All potentials are given with respect to this reference electrode.

Cyclic voltammograms (CV) for each electrode were recorded in 0.2 M HNO_3 by scanning from −0.163 to 0.240 V five times. Three replicates were conducted for this procedure to condition the electrode for further use. Accumulation was at open circuit potential for 2 min. Accumulation procedures for each electrode (pure carbon paste; silica-modified; cinnabar-modified) were at the following Hg^{2+} concentrations: 0 M, 5.0×10^{-5} M, 2.5×10^{-4} M, 1.0×10^{-3} M. At the conclusion of the accumulation period, the electrode was rinsed well with water. Adsorbed Hg^{2+} was reduced to Hg^0 in a 1 min conditioning period at 0.163 V. Anodic stripping voltammograms (ASV) were recorded in 0.2 M HNO_3 by scanning from −0.163 to 0.240 V at 0.01625 V/s in the square wave mode immediately following the conditioning period. Scans were limited to this region because an irreversible reaction appeared to occur in the 0.3 V region for the cinnabar-modified electrode which may reflect a change in oxidation state of the cinnabar. Walcarius et al. (1999) found that all of the Hg accumulated on a carbon paste electrode was removed during anodic stripping, and that the electrode could be reused without significant degradation. This was assumed to be the case for the electrodes employed in the present study, and three replicates were performed in immediate succession for each concentration. Experiments were performed from low to high concentration. ASV peak currents were compared among Hg^{2+} concentrations and electrode types.

3. Results

3.1. Dissolution of HgS

Sulfate was produced in all batch reactors (Fig. 2a–e). For experimental conditions refer to Table 1. Initial SO_4^{2-} measurements ranged from 10 μM in reactor C3 (Fig. 2e) to 100 μM in reactor C2 (Fig. 2d). Sulfate concentration increased rapidly in the first several hours of each experiment. Within 24 h, sulfate concentration reached ca. 200 μM in 0.43 M α-HgS batch reactors (Fig. 2a), 170 μM in most of the 0.1 M α-HgS batch reactors (Fig. 2b and d), and 150–200 μM in the 0.1 M βHgS batch reactors (Fig. 2c and e). After 24 h, SO_4^{2-} concentration in these batch reactors increased gradually for the duration of the experiments. In 0.1 M α-HgS batch reactors C1 and C2 (Fig. 2d), SO_4^{2-} concentration increased rapidly in the first 24 h, reached a maximum of 940 μM in C1 and 485 μM in C2, and then generally decreased. Final SO_4^{2-} concentrations were 240 μM in 0.43 M α-HgS batch reactors (Fig. 2a) and 190 to 475 μM in 0.1 M α-HgS batch reactors (Fig. 2b and d). In 0.1 M β-HgS batch reactors, final SO_4^{2-} concentrations were 170 to 780 μM (Fig. 2c and e).

Sulfate production trends were generally comparable between experiments in deionized water (Fig. 2a–c) and natural river water (Fig. 2d–e). Sulfate concentrations were similar for 0.43 M (Fig. 2a) and 0.1 M (Fig. 2b and d) α-HgS experiments despite differences in duration and cinnabar slurry concentration. The presence of Au had no detectable effect on SO_4^{2-} concentration, and the two experimental conditions (with Au and without Au) can be considered replicates. The pH was monitored in experiments C and D and was neutral at the beginning of both experiments. Within 3 h, batch reactors C1, D1, and D2 became alkaline (pH 8.1 to 9.1) and C2 became acidic (pH 3.5). After this point pH remained stable for the duration of the experiments.

3.2. Oxidation of sulfide

Splits of some samples from batch reactor experiment B (see Table 1 for conditions) were analyzed 3 and 6 weeks after the conclusion of the experiment. At 3 weeks, SO_4^{2-} concentrations were almost 200% of the original values. After 6 weeks, SO_4^{2-} concentrations had returned to within 10% of the original values. It was hypothesized that the changes in SO_4^{2-} concentration were due to incomplete oxidation of sulfide to sulfate in the original samples, and that dissolved sulfur equilibrium was not stable in the sample bottles. Several 2.5 mL aliquots of samples from B1 were treated with 50 μL of AR grade hydrogen

peroxide immediately after collection. Sulfate concentrations increased between 3 and 6% per 20 min in four successive analyses of H_2O_2 treated samples, indicating that the samples were not initially fully oxidized.

ATR-IR spectroscopy of α-HgS from batch reactor B1 revealed multiple, overlapping infrared absorption bands in the 975–1200 cm^{-1} region resulting from surface species (Fig. 3, spectrum a). Thiosulfate likely contributes to peaks in the 1010 and 1150 cm^{-1} regions, and the shoulder at 975 cm^{-1} may correspond to sulfate. Awatani and McQuillan (1998) have determined by ATR spectroscopy that the photocorrosion of cadmium sulfide produces $S_2O_3^{2-}$ (1152 and 1005 cm^{-1}) as a strongly adsorbed intermediate which gradually oxidizes to weakly adsorbed SO_4^{2-} (1107, 1060, and 970 cm^{-1}), and spectra suggest that similar surface species are present on batch reactor cinnabar in this work.

Strong infrared absorptions are present at 1145 cm^{-1} and 1014 cm^{-1} for the freshly prepared HgS (Fig. 3, spectrum b). These absorptions were assigned to $S_2O_3^{2-}$, and a solution spectrum of 0.1 M $Na_2S_2O_3$ is presented for comparison (Fig. 3, spectrum c). Coordinated $S_2O_3^{2-}$ produces infrared absorptions in the 1005–1012 cm^{-1} and 1150–1170 cm^{-1} ranges by monodentate binding (Gabelica, 1979). Infrared absorptions were also present at 1423 cm^{-1} and 882 cm^{-1} and were assigned to carbonate based on the broad infrared absorptions in the 1410–1460 cm^{-1} region and sharp infrared absorptions in the

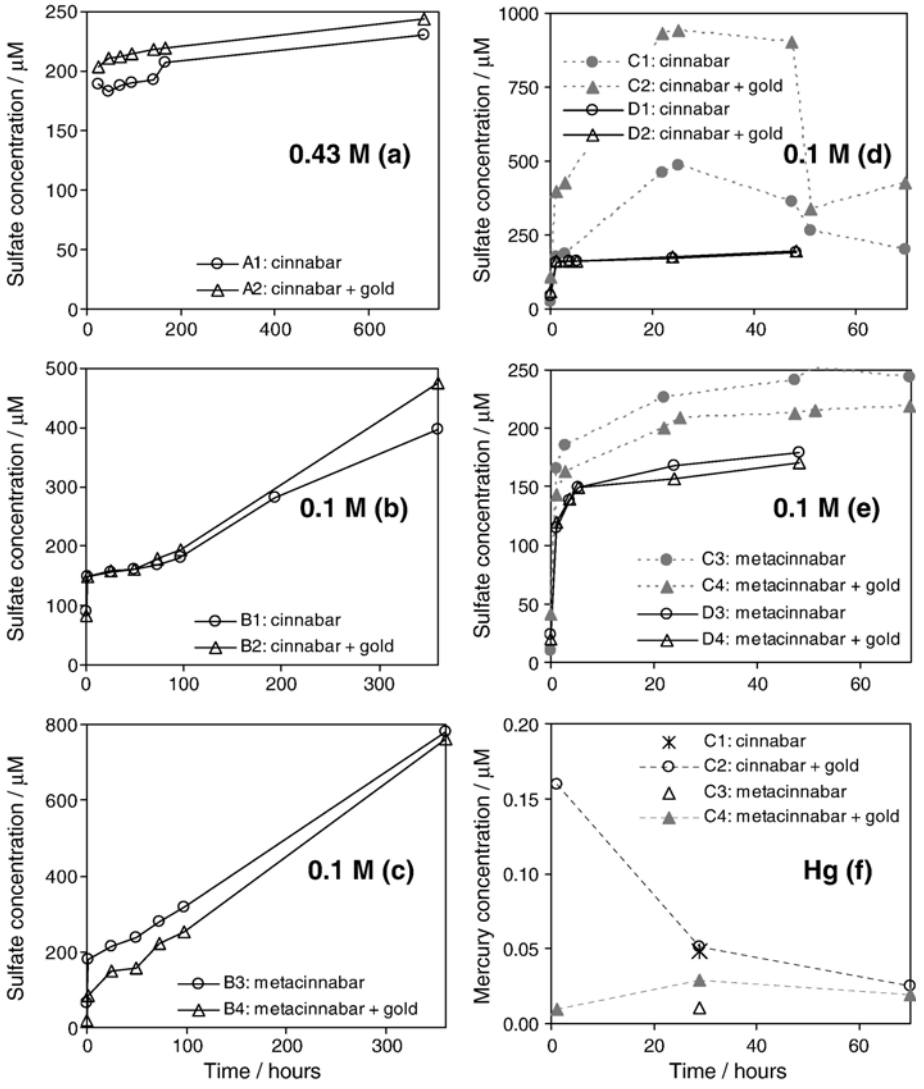

Fig. 2. Batch reactor <0.45 µm aqueous samples (a) $[SO_4^{2-}]$ in experiments A1 and A2, (b) $[SO_4^{2-}]$ in B1 and B2; (c) $[SO_4^{2-}]$ in B3 and B4; (d) $[SO_4^{2-}]$ in C1, C2, D1, D2; (e) $[SO_4^{2-}]$ in C3, C4, D3, and D4; and (f) [Hg] in C1, C2, C3, and C4. For experimental conditions refer to Table 1.

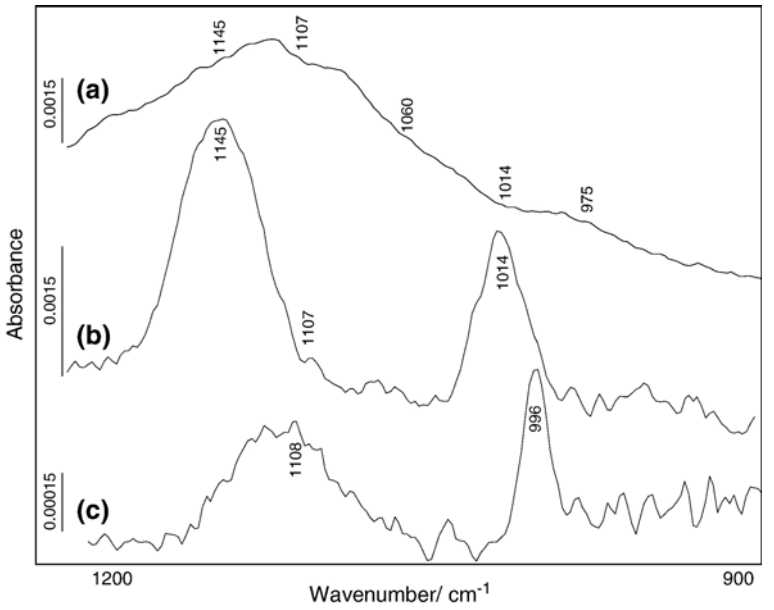

Fig. 3. Internal reflection infrared spectra of (a) α-HgS particle film prepared from drying 250 μL of a 100× dilution of slurry from batch reactor B1; (b) HgS particle film prepared from drying 250 μL of a freshly prepared 2×10^{-3} M colloidal sol; (c) 10^{-4} M $Na_2S_2O_3$ solution. Reference spectra are of the bare ZnSe prism for (a) and (b), and deionized water on the ZnSe prism for (c).

830–870 cm^{-1} region characteristic of metal carbonates (White, 1974). The absorption at 1107 was assigned to adsorbed SO_4^{2-} (Awatani and McQuillan, 1998).

Some of the surface $S_2O_3^{2-}$ was easily removed from the HgS when water and 10^{-3} M NaOH were pumped over the film. After 5 min of contact with a 10^{-4} M $Na_2S_2O_3$ solution pumped over the film, absorptions appeared at 1173 and 1011 cm^{-1}. Absorptions in these regions reached a maximum after 20 min of contact with the solution, after which point the magnitude of absorbance gradually decreased for both peaks. Sharp decreases in magnitude of absorbance were observable at 60 min when the 10^{-4} M $Na_2S_2O_3$ solution was replaced with water.

A particle film of HgS was examined by ATR-IR spectroscopy immediately after drying (Fig. 4, spectrum a). The film was subsequently exposed to the atmosphere for 90 min, and infrared spectra were collected again (Fig. 4, spectrum b). Strong infrared absorptions are apparent in both spectra at 1140 cm^{-1}, 1006 cm^{-1}, and 932 cm^{-1}. Absorptions at 932 cm^{-1} are similar to those produced by antisymmetric S–O stretch of the sulfite (SO_3^{2-}) ion at 961 cm^{-1} (Nakamoto, 1963). Absorbances are significantly greater in the latter spectrum (Fig. 4, spectrum b) for the peaks corresponding to adsorbed $S_2O_3^{2-}$.

3.3. Hg mobilized by HgS dissolution

Approximately 50 μmol (10 mg) of Hg is expected per 250 mL batch reactor if Hg is released into solution at a 1:1 molar ratio with SO_4^{2-}. Dissolved (<0.45 μm) Hg concentration decreased by 87% from 0.16 μM to 0.02 μM during the experimental period in 0.1 M cinnabar batch reactors (Fig. 2f). Dissolved Hg concentration increased by 100% from 0.01 μM to 0.02 μM during the experimental period in 0.1 M metacinnabar batch reactors (Fig. 2f). The highest concentration recorded was 0.16 μM (4.0×10^{-2} μmol Hg) (Fig. 2f; Table 1).

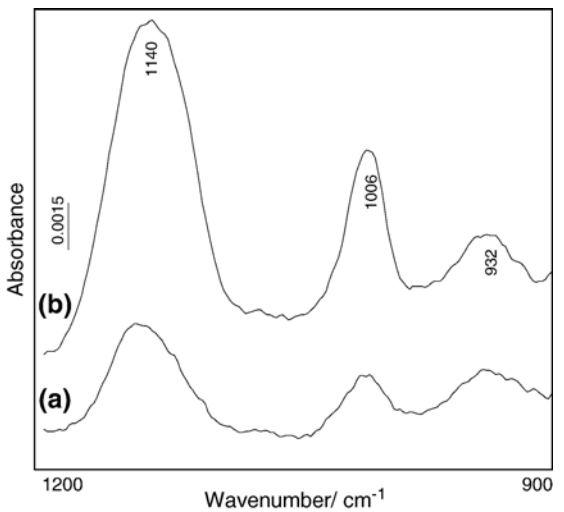

Fig. 4. Internal reflection infrared spectra of (a) the HgS particle film immediately following 30 min of drying in vacuum desiccator, and (b) after 90 min of exposure to air. Reference spectra are of the bare ZnSe prism.

Analyses of trapped Hg volatilized during sparging indicate that between 5.0×10^{-2} and 1.0×10^{-1} μmol of Hg may be lost from each batch reactor throughout the course of the experiment (Table 1), and the larger value was used to estimate the amount of Hg inferred to be lost from each batch reactor. Between 7.9×10^{-7} and 4.7×10^{-6} μmol of Hg was associated with Au in reactors containing Au foil (Table 1). The larger value was used to estimate the total amount of Hg inferred to be associated with Au in the batch reactors. From these data, yearly mercury release rates were calculated.

The total amount of Hg detected in the batch reactors was between two and three orders of magnitude less than the final amount of SO_4^{2-} in each experiment (Table 1). This was the case even when the maximum recorded amount of Hg lost by volatilization was added to the maximum amount of Hg detected in aqueous samples. The same was true for Au-bearing reactors, wherein the addition of aqueous Hg, Au-associated Hg, and inferred volatilized Hg was between two and three orders of magnitude less than the amount of SO_4^{2-} produced.

3.4. Hg^{2+} adsorption to cinnabar

Cyclic voltammograms for the cinnabar-modified electrode were S-shaped (Fig. 5). A considerable capacitive current was observed for both electrodes, although this was smaller for the pure carbon paste electrode. Two peaks suggestive of Hg desorption from the electrode occur in the anodic stripping voltammograms (ASVs) which were obtained immediately following 2 min of accumulation of Hg^{2+} on the cinnabar-modified electrode (Fig. 6). Peaks also occur at the same potential in ASVs obtained after accumulation of the maximum Hg^{2+} concentration on the pure carbon paste electrode (Fig. 6), and after accumulation of the intermediate Hg^{2+} concentration on the silica-modified electrode.

Peak currents scale with Hg^{2+} concentration for the cinnabar-modified electrode (Table 2). Peak currents for the carbon paste electrode and silica-modified electrode

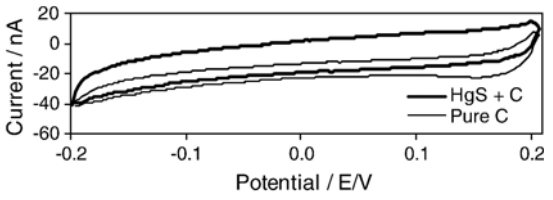

Fig. 5. Cyclic voltammograms of HgS-modified and pure carbon paste electrodes in 0.2 M HNO_3. Scans were positive-going and began at −0.163 V. The fifth scan is shown for each electrode.

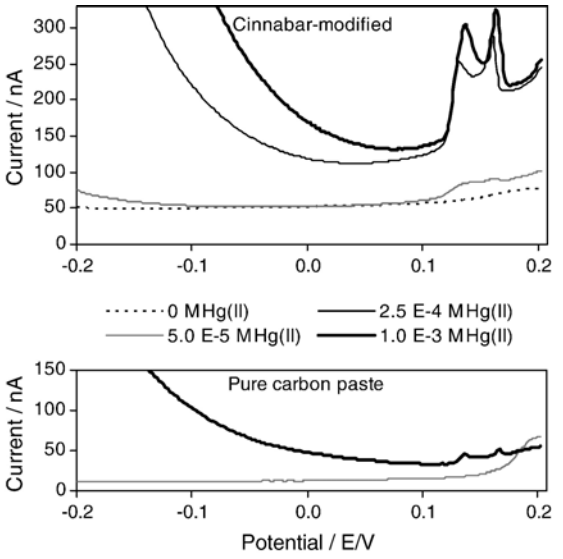

Fig. 6. Anodic stripping voltammograms of a-HgS-modified and pure carbon paste electrodes in 0.2 M HNO_3. The α-HgS-modified electrode voltammograms were following 120 s of accumulation at open circuit in 0 M, 5×10^{-5} M, 2.5×10^{-4} M, and 1×10^{-3} M Hg^{2+}. Pure carbon paste electrode voltammograms were following 120 s of accumulation at open circuit in 5×10^{-5} M and 1×10^{-3} M Hg^{2+}.

were an order of magnitude less than peak currents for the cinnabar-modified electrode after accumulation in equivalent Hg concentrations (Table 2). Peaks were reproducible with successive periods of accumulation and anodic stripping on the cinnabar-modified electrode, excepting accumulation in the highest Hg concentration. Following the initial accumulation in 1.0×10^{-3} M Hg^{2+}, the next three experiments (accumulation and anodic stripping) on the α-HgS-modified electrode did not produce peaks. When peaks reappeared on the fourth

Table 2
Peak potentials and currents for HgS-modified, silica-modified, and pure carbon paste electrode anodic stripping voltammograms

Solution $[Hg^{2+}]$/M	Electrode	Peak potential/V	Peak current/nA
5.0×10^{-5}	α-HgS-modified	0.170	2.77
		0.198	4.15
2.5×10^{-4}	α-HgS-modified	0.168	68.0
		0.196	65.8
	Silica-modified	0.162	2.66
		0.194	3.63
1.0×10^{-3}	α-HgS-modified: initial	0.174	96.4
		0.200	88.3
	α-HgS-modified: 4th replicate	0.160	3.90
		0.198	2.74
	Pure carbon paste	0.174	7.77
		0.204	7.00

experimental cycle, peak currents were ⅓ of those in the original voltammograms (Table 2). The potential of the peak previously at 0.174 V shifted to 0.160 V, and peak shape was narrower.

4. Discussion

4.1. Dissolution of HgS

Sulfate concentrations indicate that cinnabar and metacinnabar dissolve in oxygenated, agitated aqueous slurry experiments. Sulfate concentration increased for the duration of the experimental period (up to 720 h) in all batch reactors except C1 and C2 (refer to Table 1 for conditions). Similar SO_4^{2-} concentrations in 0.43 M and 0.1 M α-HgS batch experiments suggest that SO_4^{2-} production is not directly correlated with HgS slurry concentration.

Dissolution rates were calculated based on SO_4^{2-} concentration. Rates decreased by one to two orders of magnitude after 24 h, which may represent a shift from chemical to transport-controlled reactions as surface species accumulate on the HgS. Alternatively, the initial rapid phase of dissolution may reflect the removal of surface-bound SO_4^{2-} present prior to the experiment. Moses et al. (1987) described the difficulty of performing adequate SO_4^{2-} removal pretreatments for pyrite oxidation studies. They found that SO_4^{2-} was removed from the surface of pyrite in boiling acid, but that the products of oxidation in the experiment depended highly on the pretreatment method. In order to avoid the creation of surface species during a washing procedure, no pretreatments of the HgS were employed in the experiments reported here. It is assumed that any surface-bound species remaining from the chemical synthesis of HgS during manufacturing would be removed during the first 48 h, and that the dissolution rates calculated at 48 h represent the production of SO_4^{2-} due to oxidative dissolution of HgS. The rates presented here are minimum estimates based on the proportion of sulfur released from HgS that exists as SO_4^{2-}.

Data at 48 h were used in order to model long-term dissolution, and data from C1 and C2 were excluded because the rate of SO_4^{2-} production was not stable in this time frame. In 0.1 M experiments B–D, cinnabar dissolved from 2.64 to 6.16 μmol (SO_4^{2-}) m^{-2} day^{-1}, and metacinnabar dissolved from 1.20 to 1.90 μmol (SO_4^{2-}) m^{-2} day^{-1}. In 0.43 M experiment A, cinnabar dissolved from 0.71 to 0.82 μmol (SO_4^{2-}) m^{-2} day^{-1}.

Higher dissolution rates were correlated with lower HgS slurry concentrations. Dissolution rates in 0.1 M cinnabar reactors were 3–8 times higher than in 0.43 M reactors. For comparison, dissolution rates in 0.1 M metacinnabar reactors were 10–100 times higher than those reported in Barnett et al. (2001) for oxidative β-HgS dissolution by dissolved O_2. Initial metacinnabar slurry concentration in that work can be estimated as ~1 M based on the given experimental parameters. A similar phenomenon has been observed for silicate minerals (Lasaga, 1984; Lasaga et al., 1994), where dissolution rate depends on the concentration gradient, and rates decrease as the solution approaches saturation for that mineral. We suggest that this is also true for experimentally determined HgS dissolution rates, and that studies involving low HgS mineral slurry concentrations better simulate conditions downstream of cinnabar mine sites and in Hg-contaminated floodplains, as these systems are likely undersaturated with respect to HgS. While numerical values for dissolution may be somewhat dependent on mineral concentration, this problem can be avoided by comparison of relative rates at equivalent concentrations. Our results indicate that cinnabar dissolves to a greater extent than metacinnabar in oxygenated, low-flow, aquatic environments. The relative contributions of these minerals should be considered when planning remediation or analysis of α-HgS and β-HgS — bearing fluvial systems draining cinnabar mine sites.

4.2. Oxidation of sulfide

Treatment of batch reactor samples with hydrogen peroxide indicates that the samples were not fully oxidized with respect to dissolved sulfur, and that sulfur exists in multiple oxidation states in this experimental setting. Changes in dissolved sulfur oxidation state may account for the fluctuation in SO_4^{2-} concentration in experiments C1 and C2. Assays for total sulfur by ICP-OES indicated that sulfur species other than SO_4^{2-} could account for up to 50% of dissolved sulfur in samples collected from batch reactors after 48 h in experiment B. Analyses of this type at regular intervals would be useful in delineating temporal changes in dissolved sulfur redox state during sulfide mineral oxidative dissolution.

ATR-IR spectroscopy of thin particle films of α-HgS from batch reactor experiments revealed the presence of multiple absorption bands suggestive of adsorbed SO_4^{2-} and $S_2O_3^{2-}$. Infrared spectra of thin particle films of freshly precipitated HgS produced absorption bands indicative of monodentate-bound $S_2O_3^{2-}$ during exposure of the film to air and water. Absorbances in these band regions increased during contact of the HgS with a 10^{-4} M $Na_2S_2O_3$ solution, and during prolonged exposure of the film to air. We propose that $S_2O_3^{2-}$

sorbs to HgS by monodentate binding to surface Hg ions. Infrared spectral data obtained while the HgS film was in contact with the 10^{-4} M $Na_2S_2O_3$ solution indicate that $S_2O_3^{2-}$ adsorption to HgS reaches a maximum, and the $S_2O_3^{2-}$ is slowly desorbed. We suggest that $S_2O_3^{2-}$ is removed from the HgS surface by complexation. The mercury (II) thiosulfate complex is soluble and may exist as $[Hg(S_2O_3)_2]^{2-}$ or as $[Hg(S_2O_3)_3]^{4-}$ (Bailar et al., 1973). Formation constants have been calculated to be $\log K°_2 = 29.18$ for the former and $\log K°_3 = 30.3$ for the latter at zero ionic strength (Nyman and Salazar, 1961). We present the above described spectral data as evidence for $S_2O_3^{2-}$ as a weakly adsorbed intermediate product of mercuric sulfide oxidation, similar to intermediates formed during oxidation of pyrite (Goldhaber, 1983), galena (Chernyshova, 2003), and cadmium sulfide (Awatani and McQuillan, 1998).

Moses et al. (1987) give the following reaction for the oxidation of sulfur intermediates in the context of pyrite oxidation:

$$S_nO_6^{2-} + S_2O_3^{2-} \leftrightarrow S_{n+1}O_6^{2-} + SO_3^{2-}$$

According to those authors, the reaction tends to go to the right at pH < 7 and to the left at pH > 7. Based on this reaction and spectroscopic observations, $S_2O_3^{2-}$ must be considered as a component in alkaline batch reactors, although the extent to which $S_2O_3^{2-}$ contributes is not known. Sulfate concentration provides an underestimate of mercuric sulfide dissolution in this setting, and the dissolution rates given above are minimum values.

4.3. Fate of Hg mobilized by HgS dissolution

Mercury released from oxidative dissolution of HgS is environmentally significant. Release rates were calculated from batch reactor Hg data for gold-associated, volatilized, and aqueous Hg samples. The Hg release rates determined here were 6.45 nmol (Hg) m^{-2} day^{-1} from cinnabar, and 2.29 nmol (Hg) m^{-2} day^{-1} from metacinnabar. On the basis of this work, cinnabar is predicted to release 0.47 mg (Hg) m^{-2} y^{-1} and metacinnabar is predicted to release 0.17 mg (Hg) m^{-2} y^{-1}. Cinnabar and metacinnabar must be regarded as possible sources of dissolved Hg in settings similar to the oxidative environment modeled here.

Mercury release rates were similar among experiments conducted with deionized water (A, B) and with river water (C, D), indicating that the phenomena observed here are not a direct effect of dissolved organic matter (DOM) content. Ravichandran et al. (1998) found that no Hg was released (detection limit 2.5 nM) during α-HgS dissolution experiments in distilled water, in the presence or absence of O_2. Waples et al. (2005) reported similar results (Hg detection limit 0.05 μg) in the absence of fresh O_2. In the presence of DOM, Hg release rates in that work were an order of magnitude greater than those observed here. The effect of DOM on HgS dissolution may be governed by redox conditions, and oxidative dissolution mechanisms may overshadow or inhibit any influence of DOM. As suggested by Waples et al. (2005), various sites on the DOM may play different roles in enhancing dissolution on the HgS surface, and in forming Hg–DOM complexes. It is possible that high concentrations of DOM may contribute to release of surface-bound Hg from HgS by the formation of Hg–DOM complexes, even when the predominating dissolution mechanism is oxidation by dissolved O_2.

Contributions of Hg from natural dissolution of α-HgS and β-HgS should be considered when establishing background Hg levels in contaminated catchments. For example, Ganguli et al. (2000) have estimated that 1.5 kg Hg yr^{-1} is discharged in waters draining the New Idria mine, California Coast Range. Results from the present study suggest that the Hg flux from the New Idria site is likely due to contributions from Hg-rich tailings resulting from historical ore processing, and from natural dissolution of α-HgS and β-HgS deposits. Domagalski (2001) has documented elevated Hg concentrations in the Sacramento River region, California, which result from gold mining and α-HgS deposits. The historical anthropogenic input of Hg for Au amalgamation may be superimposed on elevated background Hg levels resulting from detrital α-HgS dissolution. The Hg released from HgS may undergo changes in speciation and bioavailability in downstream environments. In Hg-contaminated anoxic settings, sulfate reducing bacteria have been implicated in the formation of highly toxic methylmercury (CH_3Hg^+) from Hg^{2+} (Compeau and Bartha, 1985). The methylation of HgS-derived Hg^{2+} has been observed at Clear Lake, California, where HgS-rich tailings from the adjacent Sulphur Bank Mercury Mine Superfund site have resulted in 15.9 μg kg^{-1} CH_3Hg^+ in surficial lake sediments (Suchanek et al., 1998).

The amount of Hg released by oxidative HgS dissolution in this study is sufficient to form natural Au–Hg amalgam. Dissolved Hg concentration in batch reactor samples (Fig. 2f) was an order of magnitude higher than in a simulated Au placer described in Miller et al. (2002). In that study, 2.5 nM dissolved Hg^0 amalgamated with Au up to 0.48 wt.% over 14 days.

Mercury was detected in association with the Au in batch reactors in the present study, although the speciation of the Au-associated Hg is not known. Experiments of longer duration could produce Au-associated Hg concentrations detectable by electron microprobe in order to assess whether Au–Hg amalgam is formed. Mercury is predicted to amalgamate with Au consequent to HgS dissolution, if the HgS-derived Hg^{2+} is reduced. Natural Au–Hg amalgam may form in settings such as the Nevis and Nokomai Rivers in Central Otago, New Zealand, where detrital α-HgS is found in Au-bearing placers (Youngson et al., 2002), and in other alluvial Au and mercuric sulfide-bearing systems such as Cache Creek in the Sacramento River watershed, California (Domagalski et al., 2004), and the Carson River, Nevada (Lechler et al., 1997). However, the Au–Hg amalgam has been observed to be unstable over a 150 year time scale (Lechler et al., 1997), and the Hg temporarily immobilized by Au amalgamation may be susceptible to remobilization to the environment.

Although the amount of Hg mobilized by α-HgS and β-HgS dissolution is significant, the majority of the Hg is not released. In the present study, the total amount of Hg detected in batch reactors was at least two orders of magnitude less than the final amount of SO_4^{2-}. The proportion of Hg that is not mobilized during HgS dissolution may sorb to the HgS surface.

4.4. Hg^{2+} adsorption to cinnabar

Barnett et al. (2001) suggest the following reaction for oxidative dissolution of metacinnabar and adsorption of Hg^{2+}, wherein surface sulfhydryl groups are indicated by ≡S–H:

$$HgS(s) + 2{\equiv}S{-}H + 2O_2(aq) \leftrightarrow ({\equiv}S{-})_2Hg + SO_4^{2-} + 2H^+$$

Batch reactors in the present work provide evidence in support of surface-bound Hg. However, the accompanying proton production was only observed in one batch reactor experiment, and several experiments were in fact alkaline.

Anodic stripping voltammogram (ASV) peak currents were used to assess the relative propensity of adsorption of Hg^{2+} to the electrode materials used in this experiment. The specific surface area of the silica is more than two orders of magnitude greater than that of the cinnabar. If adsorption of Hg^{2+} was equal among electrode materials, we would expect greatest adsorption on the silica-modified electrode. However, ASV peak currents are largest for the cinnabar-modified electrode at all concentrations (Fig. 7). In this experiment, cinnabar is a superior adsorbent of Hg^{2+} compared to silica and carbon paste.

Peak shape can be used to assess the type of interaction between the electrode and the solution. The peaks at lower potential are wider and may be indicative of chemical interaction between the electrode material and Hg^{2+} (Fig. 6). In the case of the cinnabar-modified electrode, partial bond formation could result in the gradual desorption of Hg^{2+} from the electrode surface evident in the peak at 0.17 V. The peak at higher potential is narrower and may reflect a physical, charge-based interaction which is easily reversed during anodic stripping. This hypothesis is also relevant in the context of a decrease in peak width observed after four replications of 1.0×10^{-3} M Hg^{2+} accumulation on the cinnabar electrode. Saturation of the electrode or a change in mode of sorption may occur following the initial accumulation at high concentration. While this method does not elucidate the mechanisms of Hg^{2+} uptake, we suggest that it is an efficient means of assessing in situ the propensity of Hg^{2+} to adsorb to HgS preliminary to further spectroscopic study.

Dissolution of HgS must be considered when calculating the total load of Hg to catchments containing α-HgS mines and natural deposits or authigenic β-HgS. However, the contribution of HgS-derived Hg to the system is somewhat mitigated by the adsorption of Hg^{2+} to the HgS surface. Cinnabar and metacinnabar must be viewed as both sources of, and sinks for dissolved mercury in fluvial settings. In order to determine the long-term environmental significance of Hg^{2+} immobilization by HgS, the mechanisms and factors controlling

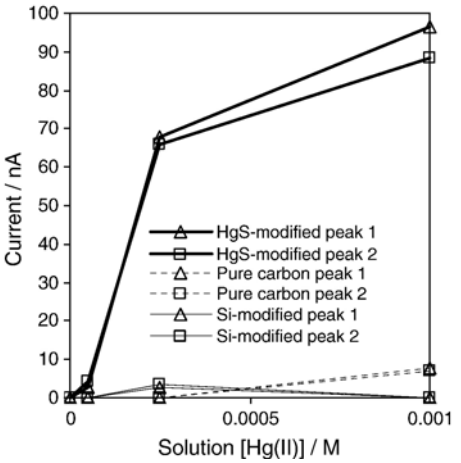

Fig. 7. Anodic stripping voltammogram peak currents as a function of Hg^{2+} concentration accumulated on HgS-modified electrode, silica-modified electrode, and pure carbon paste electrode.

this adsorption must be elucidated. Perturbations in pH, ionic strength, DOM content, and other chemical parameters in the aquatic system may affect the stability of the adsorbed Hg^{2+}, and further work is necessary to identify the conditions favorable for adsorption or desorption.

5. Conclusions

Natural dissolution of cinnabar and metacinnabar can be expected in oxidative, fluvial environments. In 0.1 M oxygenated batch reactor experiments, monitoring of SO_4^{2-} concentration indicated that cinnabar dissolved from 2.64 to 6.16 μmol (SO_4^{2-}) m^{-2} day^{-1} and metacinnabar dissolved from 1.20 to 1.90 μmol (SO_4^{2-}) m^{-2} day^{-1}. Experiments were characterized by an initial phase during which dissolution rates were two orders of magnitude higher, likely due to removal of initially present surface-bound SO_4^{2-}. Treatments of batch reactor samples with H_2O_2 suggest that dissolved sulfur exists in batch reactors at lower oxidation states in addition to SO_4^{2-}. Oxidative degradation of HgS was observed by ATR-IR spectroscopy of thin particle films. Monodentate-bound $S_2O_3^{2-}$ was identified on the HgS surface based on strong absorption bands in the 1140–1145 cm^{-1} and 1006–1014 cm^{-1} regions, confirming this species as an intermediate oxidation product of HgS. Our work indicates that SO_4^{2-} concentrations provide a minimum estimate of HgS dissolution. Even the lowest metacinnabar dissolution rates observed here are two orders of magnitude higher than would be expected based on previous studies of β-HgS solubility by Barnett et al. (2001), suggesting that experimentally determined HgS dissolution rates may be to some extent concentration-dependent.

Environmentally significant quantities of Hg are susceptible to mobilization from cinnabar and metacinnabar. Based on oxidative dissolution rates observed here, cinnabar may release 0.47 mg (Hg) m^{-2} y^{-1}, and metacinnabar may release 0.17 mg (Hg) m^{-2} y^{-1}. Higher dissolution rates were correlated with lower experimental HgS concentrations, indicating that Hg mobilization may not scale directly with the size or concentration of the HgS source. The mobilization of Hg from α-HgS and β-HgS likely contributes to naturally elevated background Hg levels even in catchments containing small quantities of these minerals. The environmental severity and identity of the final products of HgS dissolution depend upon the other components of the system. The Hg mobilized by HgS dissolution likely undergoes changes in speciation in downstream environments, and it may form natural Au–Hg amalgam in the presence of a suitable reducing agent. Much of the Hg produced by HgS dissolution may be immobilized by adsorption to HgS. The rate of Hg mobilization due to oxidative HgS dissolution was two orders of magnitude lower than the rate of SO_4^{2-} production in the present work. Adsorption of Hg^{2+} to α-HgS was detected in situ. Anodic stripping voltammogram peak currents obtained using a modified carbon paste electrode following accumulation in Hg^{2+} demonstrate that Hg^{2+} adsorbs more readily to cinnabar than to silica or carbon. Peak shape indicates that Hg^{2+} adsorption to α-HgS may be governed by both chemical and physical, charge-based interactions. The controlling factors, extent, and stability of the adsorbed Hg must be identified in order to determine the long-term environmental significance of Hg^{2+} immobilization by adsorption to metacinnabar and cinnabar.

Acknowledgements

We gratefully acknowledge the support from the University of Otago, the University of Otago Research Committee, the Rotary Foundation, and the New Zealand Foundation for Research, Science, and Technology. We thank John Watson, David Barr, Damian Walls, Lorraine Paterson, Jim Metson, and Ron Etzion for assistance with analyses, and Barry Anderson and Keith Hunter for technical support and equipment. We are also grateful to the editor and two anonymous reviewers for comments which improved the manuscript.

References

Awatani, T.M., McQuillan, A.J., 1998. Adsorbed thiosulfate intermediate of cadmium sulfide aqueous photocorrosion detected and characterized by in situ infrared spectroscopy. Journal of Physical Chemistry B 102, 4110–4113.

Bailar Jr., J.C., Emeleus, H.J., Nyhom, R., Trotman-Dickenson, A.F., 1973. Comprehensive Inorganic Chemistry, 3. Pergamon Press, Oxford.

Barnett, M.O., Turner, R.R., Sanger, P.C., 2001. Oxidative dissolution of metacinnabar (β-HgS) by dissolved oxygen. Applied Geochemistry 16, 1499–1512.

Brandon, N.P., Francis, P.A., Jeffrey, J., Kelsall, G.H., Yin, Q., 2001. Thermodynamics and electrochemical behavior of Hg–S–Cl–H_2O systems. Journal of Electroanalytical Chemistry 497, 18–32.

Burkstaller, J.E., McCarty, P.L., Parks, G.A., 1975. Oxidation of cinnabar by Fe(III) in acid mine waters. Environmental Science and Technology 9 (7), 676–678.

Chernyshova, I.V., 2003. An in situ FTIR study of galena and pyrite oxidation in aqueous solution. Journal of Electroanalytical Chemistry 558, 83–98.

Collins, C.R., Sherman, D.M., Ragnarsdottir, K.V., 1999. Surface complexation of Hg^{2+} on goethite: mechanism from EXAFS spectroscopy and density functional calculations. Journal of Colloid and Interface Science 219, 345–350.

Compeau, G.C., Bartha, R., 1985. Sulfate-reducing bacteria: principle methylators of mercury in anoxic estuarine sediment. Applied and Environmental Microbiology 50 (2), 498–502.

Dickson, F.W., Tunell, G., 1959. Stability relations of cinnabar and metacinnabar. American Mineralogist 44 (5–6), 471–488.

Domagalski, J., 2001. Mercury and methylmercury in water and sediment of the Sacramento River Basin, California. Applied Geochemistry 16, 1677–1691.

Domagalski, J.L., Alpers, C.N., Slotton, D.G., Suchanek, T.H., Ayers, S.M., 2004. Mercury and methylmercury concentrations and loads in the Cache Creek watershed, California. Science of the Total Environment 327, 215–237.

Gabelica, Z., 1979. Compounds containing cadmium and thiosulfate ions. Infrared and Raman investigation of the structural behavior of the $S_2O_3^{2-}$ ion in cadmium thiosulfate dehydrate, $CdS_2O_3{\cdot}2H_2O$. Chemical Letters 1419.

Ganguli, P.M., Mason, R.P., Abu-Saba, K.E., Anderson, R.S., Flegal, A.R., 2000. Mercury speciation in drainage from the New Idria mercury mine, California. Environmental Science and Technology 34, 4773–4779.

Gill, G.A., Bruland, K.W., 1990. Mercury speciation in surface freshwater systems in California and other areas. Environmental Science and Technology 24, 1392–1400.

Gill, G.A., Fitzgerald, W.F., 1987. Picomolar mercury measurements in seawater and other materials using stannous chloride reduction and 2-stage gold amalgamation with gas phase detection. Marine Chemistry 20 (3), 227–243.

Goldhaber, M.B., 1983. Experimental study of metastable sulfur oxyanion formation during pyrite oxidation at pH 6–9 and 30 °C. American Journal of Science 283, 193–217.

Kim, C.S., Rytuba, J.J., Brown Jr., G.E., 2004. Geological and anthropogenic factors influencing mercury speciation in mine wastes: an EXAFS spectroscopy study. Applied Geochemistry 19, 379–393.

Lacerda, L.D., 1997. Global mercury emissions from gold and silver mining. Water, Air, and Soil Pollution 97, 209–221.

Lasaga, A.C., 1984. Chemical kinetics of water–rock interactions. Journal of Geophysical Research, B 6, 4009–4025.

Lasaga, A.C., Soler, J.M., Ganor, J., Burch, T.E., Nagy, K.L., 1994. Chemical weathering rate laws and global geochemical cycles. Geochimica et Cosmochimica Acta 58 (10), 2361–2386.

Lechler, P.J., Miller, J.R., Hsu, L.C., Desilets, M.O., 1997. Mercury mobility at the Carson River Superfund Site, west-central Nevada, USA: interpretation of mercury speciation data in mill tailings, soils, and sediments. Journal of Geochemical Exploration 58, 259–267.

Miller, J.W., Callahan, J.E., Craig, J.R., 2002. Mercury interactions in a simulated gold placer. Applied Geochemistry 17, 21–28.

Moses, C.O., Nordstrom, D.K., Herman, J.S., Mills, A.A., 1987. Aqueous pyrite oxidation by dissolved oxygen and ferric iron. Geochimica et Cosmochimica Acta 51, 1561–1571.

Nakamoto, K., 1963. Infrared Spectra of Inorganic and Coordination Compounds. John Wiley and Sons, Inc., New York, p. 87.

Nyman, C.J., Salazar, T., 1961. Complex ion formation of mercury(II) and thiosulfate ion. Analytical Chemistry 33 (11), 1467–1469.

Paquette, K., Helz, G., 1995. Solubility of cinnabar (red HgS) and implications for mercury speciation in sulfidic waters. Water, Air, and Soil Pollution 80, 1053–1056.

Ravichandran, M., Aiken, G.R., Reddy, M.M., Ryan, J.N., 1998. Enhanced dissolution of cinnabar (mercuric sulfide) by dissolved organic matter isolated from the Florida Everglades. Environmental Science and Technology 32, 3302–3311.

Ravichandran, M., Aiken, G.R., Ryan, J.N., Reddy, M.M., 1999. Inhibition of precipitation and aggregation of metacinnabar (mercuric sulfide) by dissolved organic matter isolated from the Florida Everglades. Environmental Science and Technology 33, 1418–1423.

Rytuba, J.J., 2003. Mercury from mineral deposits and potential environmental impacts. Environmental Geology 43, 326–338.

Rytuba, J.J., Klein, D., 1986. Almaden type mercury deposits Model 27b. USGS open file report, pp. 95–831.

Suchanek, T.H., Mullen, L.H., Lamphere, B.A., Richerson, P.J., Woodmansee, C.E., Slotton, D.G., Harner, E.J., Woodward, L.A., 1998. Redistribution of mercury from contaminated lake sediments of Clear Lake, California. Water, Air, and Soil Pollution 104, 77–102.

Tauson, V.L., Akimov, V.V., 1997. Introduction to the theory of forced equilibria: general principles, basic concepts, and definitions. Geochimica et Cosmochimica Acta 61 (23), 4935–4943.

U.S.EPA, 1997. Mercury Study Report to Congress, EPA-453/R-97-003. U.S. Environmental Protection Agency, Washington D.C.

Walcarius, A., Devoy, J., Bessiere, J., 1999. Electrochemical recognition of selective mercury adsorption on minerals. Environmental Science and Technology 33, 4278–4284.

Waples, J.S., Nagy, K.L., Aiken, G.R., Ryan, J.N., 2005. Dissolution of cinnabar (HgS) in the presence of natural organic matter. Geochimica et Cosmochimica Acta 69 (6), 1575–1588.

White, W.B., 1974. The carbonate minerals. In: Farmer, V.C. (Ed.), The Infrared Spectra of Minerals. Mineralogical Society, London.

Xia, K., Skyllberg, U.L., Bleam, W.F., Bloom, P.R., Nater, E.A., Helmke, P.A., 1999. X-ray absorption spectroscopic evidence for the complexation of Hg(II) by reduced sulfur in soil humic substances. Environmental Science and Technology 33, 257–261.

Youngson, J.H., Woperis, P., Kerr, L.C., Craw, D., 2002. Au–Ag–Hg and Au–Ag alloys in Nokomai and Nevis valley placers, northern Southland and Central Otago, New Zealand, and their implications for placer–source relationships. New Zealand Journal of Geology and Geophysics 45, 53–69.